Int J Intell Robot Appl (2017) 1:255–270
DOI 10.1007/s41315-017-0028-4

REGULAR PAPER

Wall-climbing robot for non-destructive evaluation using impact-echo and metric learning SVM

Bing Li[1] · Kenshin Ushiroda[2] · Liang Yang[1] · Qiang Song[2] · Jizhong Xiao[1]

Received: 2 December 2016 / Accepted: 30 June 2017 / Published online: 31 July 2017

Abstract The impact-echo (IE) acoustic inspection method is a non-destructive evaluation technique, which has been widely applied to detect the defects, structural deterioration level, and thickness of plate-like concrete structures. This paper presents a novel climbing robot, namely Rise-Rover, to perform automated IE signal collection from concrete structures with IE signal analyzing based on machine learning techniques. Rise-Rover is our new generation robot, and it has a novel and enhanced absorption system to support heavy load, and crawler-like suction cups to maintain high mobility performance while crossing small grooves. Moreover, the design enables a seamless transition between ground and wall. This paper applies the fast Fourier transform and wavelet transform for feature detection from collected IE signals. A distance metric learning based support vector machine approach is newly proposed to automatically classify the IE signals. With the visual-inertial odometry of the robot, the detected flaws of inspection area on the concrete plates are visualized in 2D/3D. Field tests on a concrete bridge deck demonstrate the efficiency of the proposed robot system in automatic health condition assessment for concrete structures.

Keywords Wall-climbing robot · Non-destructive evaluation · Impact-echo · Wavelet transform · Distance metric learning · Support vector machine · Machine learning

✉ Jizhong Xiao
jxiao@ccny.cuny.edu

Bing Li
bli@ccny.cuny.edu

Kenshin Ushiroda
kenshinushiroda@gmail.com

Liang Yang
lyang1@ccny.cuny.edu

Qiang Song
songqiangty@gmail.com

[1] The Electrical Engineering Department, The City College, The City University of New York, 160 Convent Ave, New York, NY 10031, USA

[2] InnovBot LLC, Zahn Center, The City College, The City University of New York, New York, USA

1 Introduction

The aging problem of civil infrastructures including bridges, tunnels, and dams has been an important research topic of structural health monitoring (SHM). The structural integrity and deterioration levels is critical, and the failure of tracking and predicting the SHM of these constructions might lead to tremendous tragedies, such as the I-35W Mississippi River bridge collapse (Hao 2009) in 2007, United States. SHM is a significant tool to evaluate the health of these infrastructures by collecting the routine inspection data, and further analysis is performed to evaluate the sustainability of these infrastructures.

It is very challenging (Liu et al. 2014) and costly to inspect surfaces (Fig. 1), which are not easily accessible, such as building walls or bridge pillars. The current manual inspection is time consuming, expensive, and often requires the use of extensive scaffolding, leading to human safety concerns. Climbing robot with the ability to maneuver on vertical surfaces is needed to automate the inspection process, and it provides vertical mobility to allow inspections to be performed significantly faster, safer, and at a lower cost.

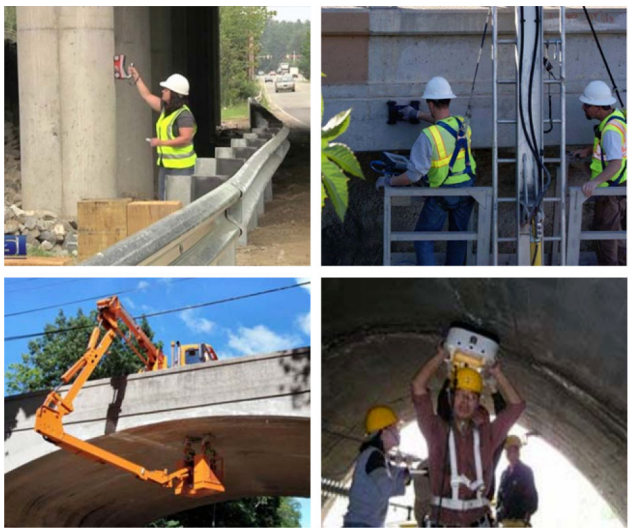

Fig. 1 Manual inspection using NDE instruments Xiao and Agrawal (2015)

In addition to the visual inspection of surface flaws, various non-destructive evaluation (NDE) technologies (McCann and Forde 2001) were developed to inspect the structural integrity and deterioration [i.e., cracks, delamination, or voids (Xiao and Agrawal 2015)] levels of the inner concrete structure, such as the approaches of ultrasound (Tan et al. 1996), ground-penetrating radar (GPR) (Daniels 2000), seismic pavement analyzer (PSA) (Gucunski and Maher 2002), IE (Sansalone and Streett 1997). Among these available NDE devices, hand-held IE is the most commonly used technology for evaluating concrete and masonry structures, since the advantages of IE technology includes easy usage, low cost, and reliability. This technology was invented by the US National Bureau of Standards and Cornell University (Sansalone and Streett 1997; Carino 2001), and was commercialized by impact-echo Instruments LLC and Olson Engineering Inc (Olson 2010), which developed the handheld 2D/3D impact-echo detection devices without automatic inspection function. In addition, the 2D view [such as B-Scan, C-Scan (Liu et al. 2004)] and volumetric view (Liu and Yeh 2012) were also researched to visualize detected IE results.

To design a NDE robot for automatic IE collection and interpretation for both horizontal plates and vertical surfaces, based on our previous research (Xiao and Agrawal 2015; Xiao et al. 2005a, b, 2006, 2015; Xiao and Sadegh 2007; Xiao and Wang 2015; Li et al. 2014), this paper proposed a novel wall-climbing robot (namely Rise-Rover) for IE NDE, and the main contributions of this paper include:

1. Designed our new generation wall-climbing robot, with the suction cups novelly embedded in the wheel track to improve both mobility and stability.
2. To the best of our knowledge, this paper newly applied the metric learning-support vector machine (ML-SVM) approach for the IE classification for concrete structures. Conventional SVM support vectors distance is considered uniformly for all features, and it causes classification inaccuracy, but ML provides an adaptive distance metric according to different classes and features.
3. The IE NDE device was deployed in our Rise-Rover for the field data collection on a concrete bridge deck with cracks, and data analysis shows the effectiveness of the proposed approaches.

The rest of the paper is organized as follows: In Sect. 2, the related works are presented. Then in Sect. 3, the overview design of the proposed NDE robot is described. Subsequently, Sect. 4 elaborates the mechatronics design of the Rise-Rover. In Sect. 5, the theoretical analysis of the IE signal using fast Fourier transform (FFT) and wavelet transform (WT), and distance ML-SVM classifier are elaborated upon. Section 6 shows the experimental results. Finally the conclusion and future work of this research are discussed in Sect. 7.

2 Related works

Impact acoustic inspection method is based on the impact sound signal generated by a small hard object knocking on the surface of concrete structures. It is the pattern of the waveforms and power spectral density (PSD) of the impact-echo signals that indicate the existence and locations of the flaws. Sansalone and Streett (1997) also points out that when the transducer is placed close to the impact point, the response is dominated by P-wave echoes, which can be analyzed by the Fourier transform technique. The PSD of the acoustic signal frequency is used as the source of the signal features, such as: the power accumulation ratio (Wu and Siegel 2000), the sound intensity ratio (Liu et al. 2007), and the area of interval PSD (Tong et al. 2008). The threshold limitation evaluation method, as a traditional approach, was applied by several researchers (Liu et al. 2007; Ito and Uomoto 1997). Although it is a simple approach, its sensitivity to the noise makes it unreliable for practical applications.

In addition to Fourier analysis on the frequency spectrum domain, Wavelet transform (WT), as a time-frequency analysis approach, became a prevalent method to interpolate underlying characteristics inside of IE signal as well as for signal de-noising (Sardy et al. 2001). The wavelet packet decomposition (WPD) was applied in the research of WICBOT (Luk et al. 2009) and the features of PSD using WPD were used for the artificial neural network

(ANN) classification. To overcome the difficulties of FT (such as to avoid phenomena of ripple and multiple-peak), an enhanced Fourier spectrum approach was presented by multiplying the Fourier spectrum with wavelet marginal spectrum (Yeh and Liu 2008). Wavelet decomposition was also applied for feature extracting and concrete full condition assessment (Zhang et al. 2016).

To automate the evaluation of SHM from NDE devices, various machine learning techniques have been applied on the extracted features from the collected signals. The overview of data-driven machine learning applications on SHM can be referred in Harley (2014), Farrar and Worden (2012), Ying et al. (2012) and Srivastava and Han (2011). For the impact-echo NDE, a few researches have applied some conventional machine learning techniques to recognize and classify the IE signals. ANN is a typical machine learning technique which has been used for the Impact acoustic signal analysis (Pratt and Sansalone 1992; Luk et al. 2009) in the past decades. The extreme learning machine (ELM) approach, as a type of feed-forward neural networks, has been newly used to explored for the IE analysis (Zhang et al. 2016). The drawbacks of ANN are that it needs a large amount of training samples, depends heavily on the empirical principles, and also the characteristics of the impact acoustic features suppress the generalization capability of ANN (Tong et al. 2008).

Support vector machine (SVM), which is based on the statistical learning theory, is characterized for classification with the capability of learning from datasets at small size, and has been applied for the IE classification such as in Tong et al. (2008) and in our previous research Li et al. (2014). Farrar and Worden (2012) chapter 11 gives more details of SVM for structural health monitoring. The SVM transfers the low dimensional feature space of IE signal into higher dimension, so that to classify the signal into different classes by maximizing the margin using a hyperplane. To find an adaptive margin threshold for different classes in the SVM, in this research we propose to use a distance metric learning (ML) approach to learn a distance measurement over the IE signal datasets. Distance learning approach was initially presented by Short and Fukunaga (1981), and ML which is proposed by Xing et al. (2003) was an earlier work for the unsupervised clustering learning. Later it was applied with SVM to learn a Mahanalobis distance for the classification (Nguyen and Guo 2008; Liu and Caselles 2011).

To successfully accomplish the automation NDE inspection task, various types of climbing robots and adhesion mechanisms are explored (Xiao et al. 2005b, 2006; Ward et al. 2013; Guan et al. 2013; Bi et al. 2012). The climbing robot from International Climbing Machines (ICM) which produces a large climbing robot using an AC vacuum pump to generate strong suction and uses rolling tread with thick foam to create a seal perimeter. It is so far one of the most mature robot prototypes that has the potential to be used in NDE inspection of civil infrastructure (Strickland 2013). The ICM robot can generate very strong adhesion on smooth and rough surfaces and overcome small surface irregularities using thick foam. However, the major weakness of this robot is that it has one vacuum chamber that requires perfect sealing enclosed by the thick foam tread. The robot falls when the vacuum breaks, and it happens when the robot crosses a ditch or deep groove/gaps, which are very common on brick/concrete walls. For the impact-echo robot, WICBOT shows a tile-wall inspection mechanical system (Luk et al. 2009), and it uses a cable driving mechanism to move along the tile wall for IE inspection.

3 System overview

The Rise-Rover climbing robot (as shown in Fig. 2) is designed to perform NDE inspection on both horizontal and vertical concrete plates, with caterpillar chain-tracks wheels to achieve fast locomotion on flat surfaces and embedded suction cups for adhesion reliability. By recording the odometry of the robot during the inspection, the IE signals are stored with regards to corresponding locations. The structure of Rise-Rover is shown in Fig. 3, with extended external sensors.

The software of Rise-Rover is running under robot operating system (ROS) Indigo platform on Ubuntu 14.04 in a Nvidia Jetson TX1 board, which is used for motion control and IE signal acquisition. The locomotion mobility of Rise-Rover is driven by four brushed wheel motors with encoders embedded, and it is in the form of differential drive since each side is actually controlled by one of the

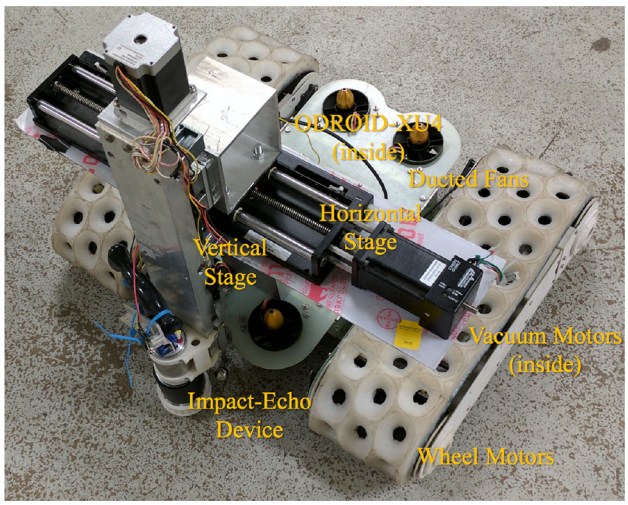

Fig. 2 IE-equipped Rise-Rover robot on concrete surface

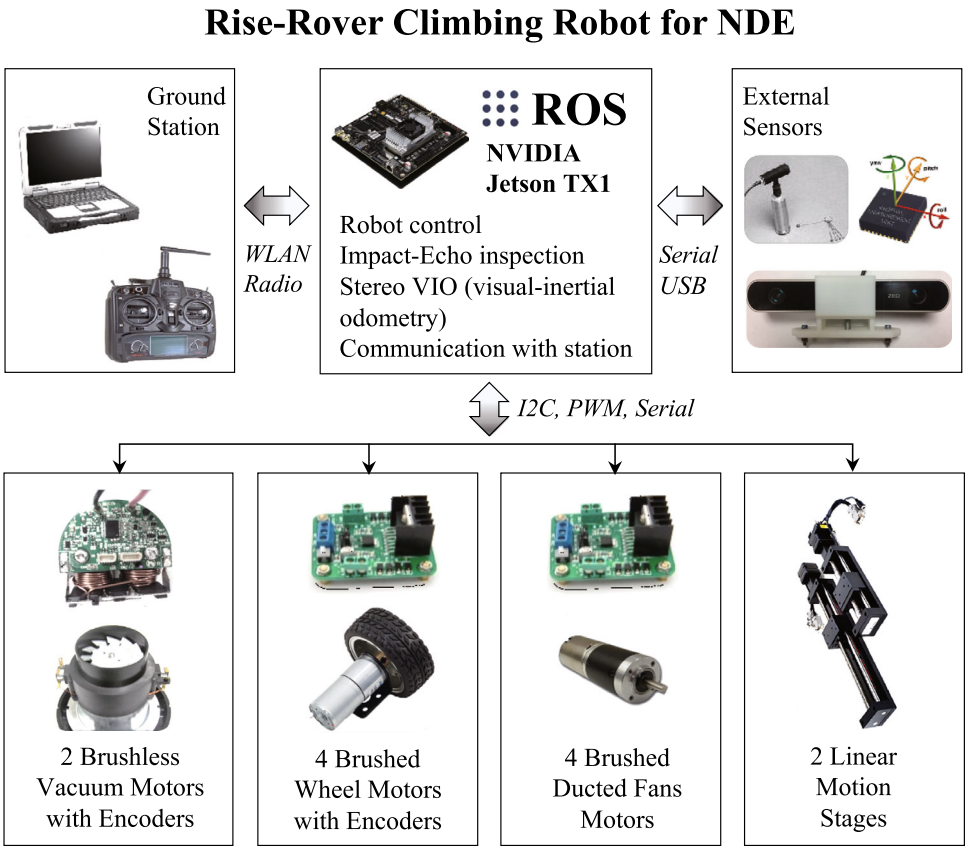

Fig. 3 Rise-Rover system configuration

pulse width modulation (PWM) channels. When the Rise-Rover detaches the vertical surface in any case, the four ducted fans are used to push the robot toward the wall. Using a ZED stereo camera and nine-axis Xsens inertial measurement unit (IMU), a stereo visual odometry (Mur-Artal and Tardós 2016) is fused with IMU using multi-state extended kalman filter (MS-EKF) is applied for positioning in the environment. The robot can be controlled by the ground station using an industrial laptop or radio controller, and the onboard camera can be enabled for image capturing and live inspection.

4 Mechatronics design

4.1 Mechanism system

Figure 4 shows the exploded view of our innovative design for Rise-Rover wall-climbing robot prototype. The robot uses two individual drivetrains on both sides and two ducted fans in the middle of the chamber.

The innovative design of the drivetrain system for Rise-Rover climbing robot is as shown in Fig. 5. The drivetrain consists of two drive wheels, a foam tread, a rotor package with air chamber and impeller, and a perforated spring steel band (belt). The backside of the foam tread is lined with the belt which provides structure and prevent deformation to the tread. The chamber seals are used to prevent/reduce the air flowing from the edge via like gaps, while the pressure valve is driven by the suction motor to extract the air so that a certain negative pressure in the chamber can be controlled by the suction motor controller based on proportional-integral-derivative (PID). The holes in the belt allow the drive wheels to pull the belt with matching teeth, and also serves as ports so that the air can be evacuated from the circular openings in the foam. The ultra-high-density foam is adaptable to surface irregularity and provides a rolling seal to the chamber. The chamber is evacuated by a 2.75-inch diameter vacuum impeller powered by a light, quiet, and high-speed brushless motor. The chamber is divided into three sections and contains two pressure valves which close upon the breaking of a seal, virtually increasing the number of independent chamber seals to three.

The rotor package is with improved features for Rise-Rover robot. The rotor package produces adhesion for the drivetrain to scale vertical walls while the high-density foam helps to reduce disturbance and muffle the impeller noise. The design had several iterations of improvement with multiple validation tests. We evaluated the relationship between impeller speed and adhesion force, and the improvement in noise/disturbance reduction. We found that

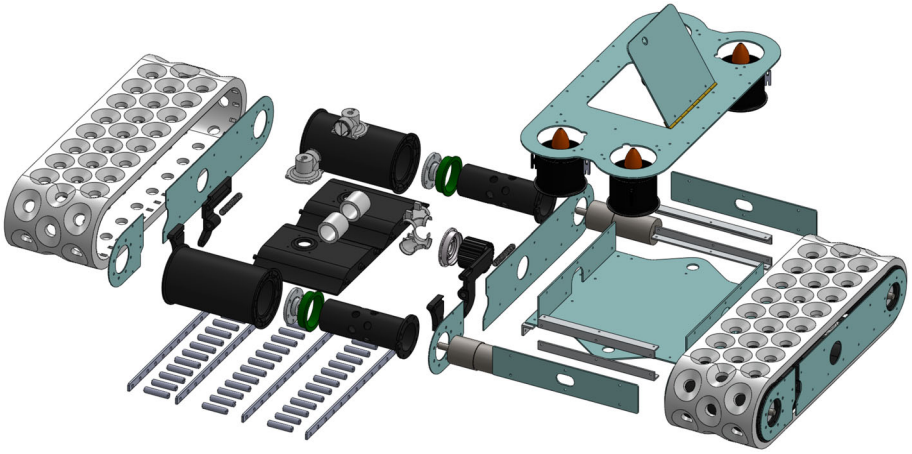

Fig. 4 Exploded view of Rise-Rover wall-climbing robot

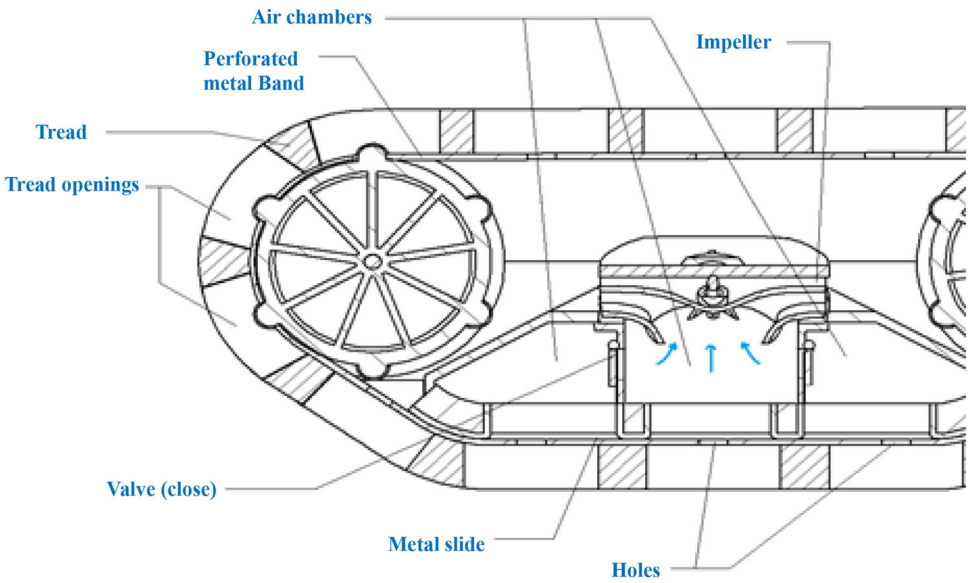

Fig. 5 The cut-away drawing of the drivetrain

it's very important for the short-delay of the suction motor control. The most critical test is to determine if the track can rotate when it is pushed against the wall with maximum suction force. The experiment comes out that the driving motor, when it is powerful enough, is able to overcome the friction on the track and provide adequate mobility. We also tested the valves function well in dividing the chamber into multiple sections for independent sealing effects.

4.2 Reliability design

For any wall-climbing robots working on the vertical space, reliability is a very critical factor. Climbing robots must be able to supply necessary adhesion force to operate on various wall surfaces, attach to a wiring harness for safety, and implement fault tolerance features to deal with deep cracks/ditches and ledges/overhangs on wall surfaces.

Since the Rise-Rover has three individual chamber seals on each tread, any straight-line gaps cannot cross all chamber seals at any given time. Thus, the robot is able to cross over ditches.

Another novel reliability design is ducted fans to push the robot in contact with vertical surface when it is suspended in midair. The thick foam tread is deformable to cope with surface irregularities that may exist. The propellers of two duct fans generate push force to allow re-adhesion of the robot against vertical walls when it loses contact with the surface. This feature is important in dealing with ledges, overhangs and other obstruction above the surface since it allows the robot to reach contact surface. It allows the robot to reach a large variety of structures. When the robot is in good contact with the wall by impeller adhesion, there is no need to activate the ducted fan. However, when the adhesion is less than required, propulsion force from the ducted fan will be helpful to compensate the deficiency. The combination of impeller

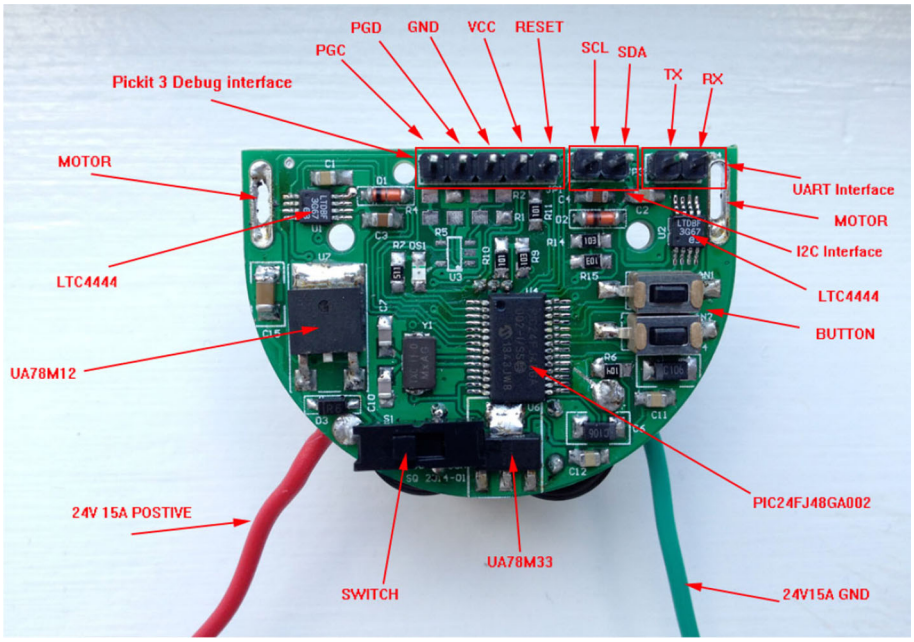

Fig. 6 High-speed brushless DC controller and driver

and propeller (duct fan) is a fault tolerant feature that makes the robot a versatile machine which is capable of scaling even on the most irregular surfaces. A cable reel will be used to feed tether to the wall-climbing robot that enhances safety, supplies power, and provides control signals to operate Rise-Rover robot and inspection sensors.

4.3 Electronics design

The Rise-Rover platform was designed initially with minimal control and sensing to reduce the mass of the overall system and simplify the electronics configuration. Rise-Rover is running on Ubuntu 14.04 ROS (Indigo) in a Nvidia Jetson TX1 board, powered by a 3-Cell, 11.1-V 1200-mAh Lithium Polymer battery. The electronic system of Rise-Rover consists of two brushless vacuum motors with encoders (up to 300 oz-in and 10K RPM), four brushed wheel motors with encoders (100 oz-in and 3K RPM), four brushed ducted fan motors (50 oz-in and 3K RPM), and a 2-linear motion stage. External sensors include an IE NDE device, a TED stereo camera, and a nine-axis Xsens IMU.

To ensure reliable adhesion for the vacuum suction system, we designed a high-speed brushless DC motor controller and driver board as shown in Fig. 6, which is with a PIC24FJ48 microcontroller unit (MCU). It is compactable in the dimension of 50 mm $\times$ 30 mm. By integrating with a onboard pressure sensor, a proportional-integral-derivative (PID) algorithm is implemented for pressure control and robust fast step response.

The robot is equipped with a set of NDE impact-echo device as shown in Fig. 3 including impactor (hardened steel spheres) which can be selected in various sizes, a cylindrical transducer and an analog-to-digital (AD) data acquisition board. The impact action is controlled by servo motor, the transducer transfers the received acoustic signal, and it was sampled by the AD board. The transducer is mounted on a 2-linear motion stage, so that the horizontal stage enables the detection points in 2D, while the vertical stage leads the transducer attaching or detaching the concrete plate surface.

5 Impact-echo inspection

After several design and test iterations, we have successfully developed our Rise-Rover prototype (Fig. 2), with impact-echo device installed on the robot (Fig. 7) to perform IE inspection. The mechanical characteristics of the IE cylindrical transducer is in the diameter around 62 mm. The diameter impacting sphere can be chosen in a series of diameter sizes from 1.5–10 mm. The transducer produces a voltage in the maximum range of 2.5 volts. More details info of IE device can be referred to Impact-Echo Users Manual[1] from Impact-Echo Instruments, LLC.

It is the patterns of the waveforms and spectra (especially the latter) that provide information about the existence and locations of flaws (cracks, voids, delamination, etc.) in concrete plates (Galt et al. 1997). The comparison of the two signals with different frequencies during the impact process is shown in Fig. 8. The reflected waveforms differ in the aspect of *d*, which is the distance between the

[1] http://www.impact-echo.com/_resources/Impact-Echo-Manual.pdf

Fig. 7 *Rectangles* from *left* to *right*: position limit switch, IE transducer and IE impactor on Rise-Rover

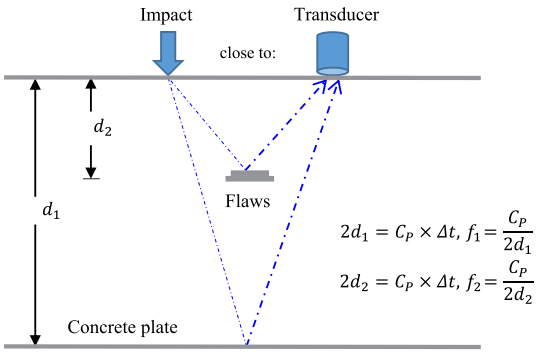

Fig. 8 Frequency and depth of two compared waves

impact knocking point and transducer. C_p is the propagation speed of the P wave in the medium.

5.1 Signal analysis

Figure 9 shows the methodology framework for the impact-echo (IE) analysis. After the IE signals are acquired and pre-processed with the de-noising, FFT and DWT are performed. Then PSD and SDW coefficients are selected as the pattern features for SVM. The distance metric learning (ML) is applied to learn the Mahalanobis distance as the marginal for the support vector distance for the hyperplane classification using semi-definite programming (SDP).

5.1.1 FFT analysis

The IE signal is sampled and stored in the form of discrete digital sequence, which we represent as a resultant below:

$$x_n = \hat{x}_n + \epsilon_n, n \in [1, ..., N], \tag{1}$$

where N is the signal sampled temporal length, $\hat{x}_n$ is the IE signal, and ϵ_n is the contaminated noise.

To reduce the influence of contaminated noise in the temporal signal, a de-noising filter is applied. For the noise with proportional distribution in the frequency spectrum (such as white noise), only the overall amplitude of the frequency spectrum is distorted. In this way, a high frequency rejected filter is applied, and the majority of the selected feature patterns are retained and distortion is suppressed.

Fourier transform (FT) is a powerful tool to analyze the signal characteristics in the frequency domain, and it has been applied conventionally to the IE analysis to determine the internal cracks and flaws of concrete structure by the peak analysis in the Fourier spectrum. a discrete-time Fourier transform (DTFT) is applied for the N-periodic temporal sequence samples, as the complex valued function shown in Eq. (2).

$$X(k) = \sum_{n=0}^{N-1} x(n) e^{-2\pi jkn/N}, \tag{2}$$

$x(n)$ is the discrete-time instant signal, $X(k)$ is the DTFT transformed frequency spectrum, and $k \in [1, ...N]$ is the real-valued discrete-frequency which is with periodicity.

The normalized power spectral density (PSD) distribution pattern of DTFT is defined as:

$$\rho(k) = \frac{X(k) \cdot X^*(k)}{\eta}, k \in [1, ...N], \tag{3}$$

where $X^*(k)$ is the conjugation of $X(k)$, and η is the normalization factor to normalize the influence of the IE strength, and is calculated by the sum of all numerator.

5.1.2 Wavelet transform

The wavelet transform (WT) is applied to extract the salient features from IE signals in this research, and it's able to analyze the signals in both temporal and scale information simultaneously, so that to capture the frequency content of sudden changes in a certain time interval.

Let's denote $W(\alpha, \zeta)$ as the WT of an IE signal $x(n)$, we have:

$$\begin{aligned} W(\alpha, \zeta) &= \eta \sum_{n=0}^{N-1} x(n) \Phi\left(\frac{n-\zeta}{\alpha}\right), \\ \eta &= \frac{1}{\sqrt{\alpha}}, \\ \alpha &= \Psi(f), \end{aligned} \tag{4}$$

where $\Phi(t)$ is the mother function of wavelet decomposition, α is the dealation parameter as a function of pseudo-frequency f, that $\alpha = \Psi(f)$ is defined corresponding to the selected wavelet function $\Phi(t)$ [which is Daubechies (dbN) Wavelets in our cases]. ζ is the wavelet translation

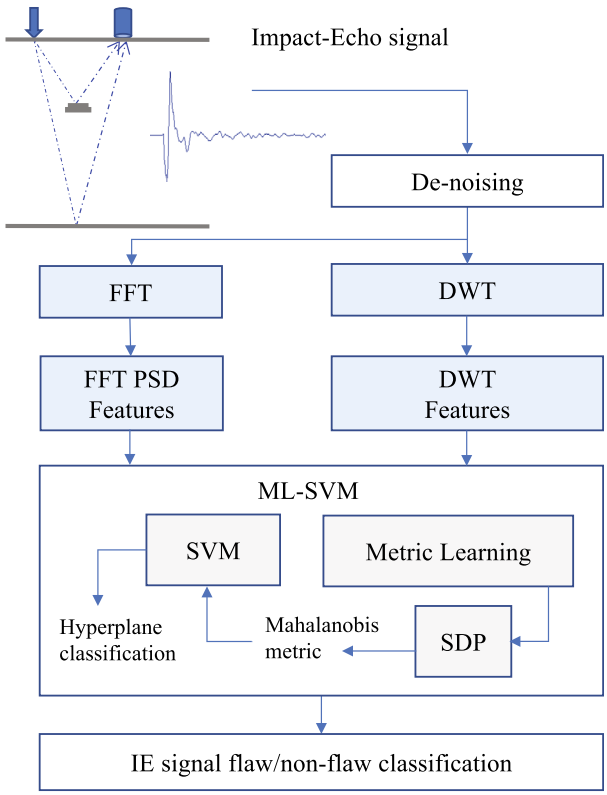

Fig. 9 Proposed methodology for the IE analysis

parameter which is the middle of N. η is the normalized factor for the unitary of each wavelet energy based on wavelet function and the pseudo-frequency f.

Figure 10 shows the IE signal and its main discrete wavelet transform (DWT) coefficients.

The density distribution of $|W(\alpha,\zeta)|^2$ is called scalogram, which represents the signal energy distribution in time and frequency domain, and the temporal variation information corresponding to f. The scalogram of an IE signal is shown in Fig. 11. The wavelet marginal spectrum (WMS) provides the pseudo-frequency f content of IE signal in time domain, and can be obtained via the scalogram by:

$$M(f) = \sum_{\alpha} |W(\alpha,\zeta)|^2 = \sum_{f=1}^{+\infty} |W(\Psi(f),\zeta)|^2. \quad (5)$$

Discrete WT decomposes the IE signal into orthonormal bases sets which are corresponding to scales or resolutions of different time and frequency. A 4-level wavelet decomposition is applied to decomposed the IE signals, and the Daubechies dbN Wavelets is applied as the mother wavelet functions (N is the vanishing moments number, and two is selected from our experimental analysis). The decomposition concept is shown in Fig. 12. Starting from $cA_0 = x(n)$ as the original temporal signal, and it's decomposed into the first-level of approximation cA_1 and detail coefficients cD_1. Then the approximation of each level is decomposed into a lower level of WT. Each approximation includes the high-scale and low-frequency components, while the detail coefficients includes the components of low-scale and the high-frequency.

5.2 Pattern extraction

Before the classification for the IE signals of various flaws, we perform the feature extraction, which indicates the underlying features of the flaws for predictive models of the metric learning SVM. Although WT is able to capture the sudden changes of the IE signal, it comes with lower frequency resolution compared with FT. In this research,

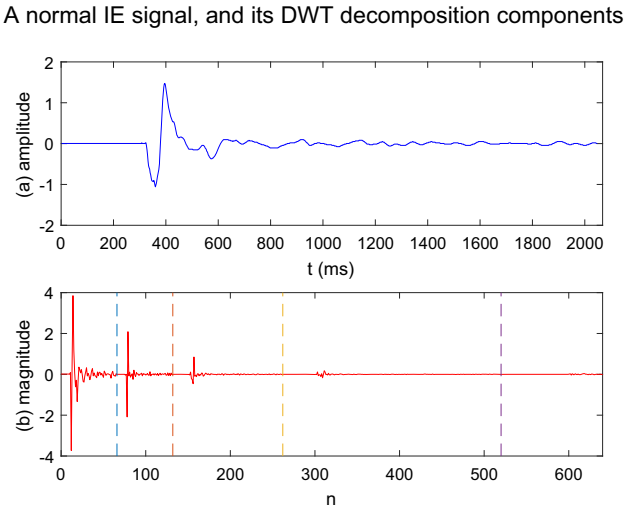

Fig. 10 IE signal and its DWT coefficients

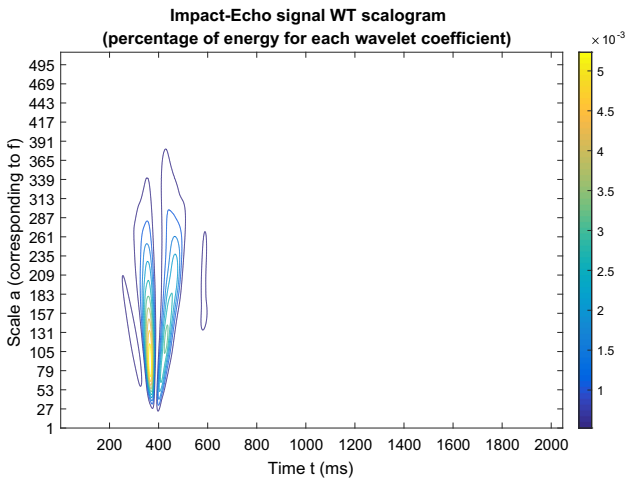

Fig. 11 IE signal scalogram

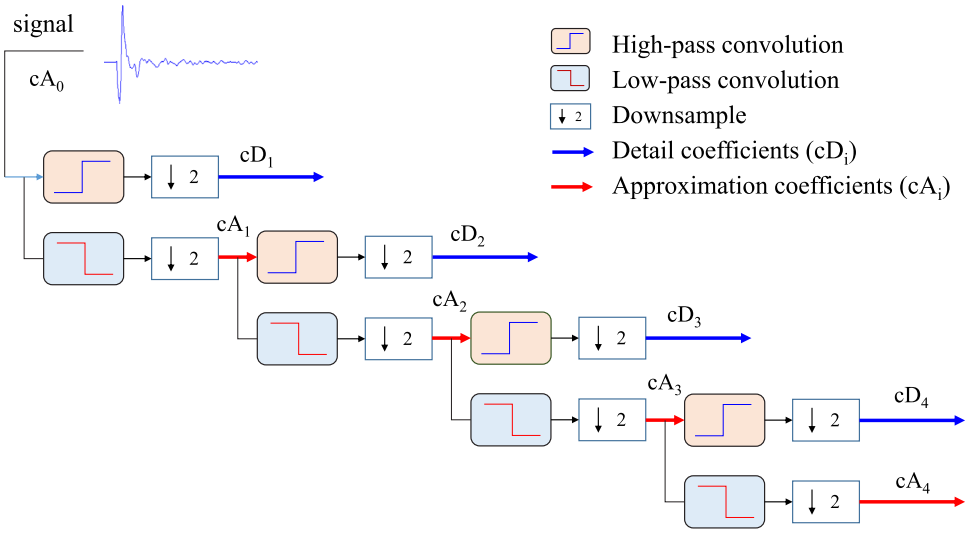

Fig. 12 WT 4-level decomposition

we proposed to combine the features of FFT and WT for the SVM training and classification.

For WT, the main components cA_4, cD_4 and cD_3 are selected for the feature extraction, since these components occupies the significant energy in PSD. For each component as well as temporal x and its FT X, we perform the features extraction.

Given a temporal signal $\{x(n)\}, n \in [1, \ldots N]$, according to Eqs. (2) and (3), we get the spectrum of the x as $X(f_k)$, $k \in [1, \ldots K]$, where K is the frequency bin number. Since the peaks in the frequency domain are significant to indicate various flaws, the followings from Eqs. (6)–(10) (with description in Table 1) are selected as the features (for each PSD) for classification. Where the total power $P = \sum_{k=1}^{K} X(f_k)$, $\bar{x} = \frac{1}{N}\sum_{n=1}^{N} x_n$ is the mean of x_n, and k_Δ indicates the threshold for spectral frequency around k_p, which is selected as the 2nd maximum peak in the PSD.

$$E = \sum_{n=1}^{N}(x_n - \bar{x})^2, \tag{6}$$

$$f_1 = \frac{\sum_{k=k_p-k_\Delta}^{K} X(f_k) f_k}{P}, \tag{7}$$

Table 1 The features from temporal signal, its FFT and WT

Features	Description
E	Signal centralized energy
f_1	Power spectral density centroid
f_2	Power spectral density std.
f_3	Power spectral density skewness
f_4	Power spectral density kurtosis

$$f_2 = \sqrt{\frac{\sum_{k=k_p-k_\Delta}^{K} x(f_k)(f_k - f_1)^2}{P}}, \tag{8}$$

$$f_3 = \frac{\sum_{k=k_p-k_\Delta}^{K} x(f_k)(f_k - f_1)^3}{(f_2)^3 P}, \tag{9}$$

$$f_4 = \frac{\sum_{k=k_p-k_\Delta}^{K} x(f_k)(f_k - f_1)^4}{(f_2)^4 P}. \tag{10}$$

For the temporal signal, for its three main FFT and WT components, we totally select 4×5 features, which are used as the characteristics for classifying the defects and flaws in the concrete plates.

5.3 Metric learning SVM

For IE flaw classification, SVM model is firstly trained with the training data set, and then is used to predict the classification of the testing datasets. The basic idea of SVM is to transform the signal into a higher dimensional space and find a hyperplane to classify the data into binary parts by maximizing the margin.

Given a set of labeled training samples $\{x_i, y_i\}, i \in [1, 2, \ldots, M]$, where $x_i \in X$ as the vector space $\Re^{\mathfrak{d}}$, $y_i \in Y$ as a set of finite labelled classes. For the case of binary classification, $Y = [-1, 1]$. M is the sample number. $\{x_i, y_i\}$ will be guaranteed to be linearly separated by SVM kernel transform, which maps the input vectors to a higher dimensions (Xiao and Wang 2015). The SVM approach aims at finding the classifier in the form of:

$$\begin{aligned} y(x) &= sign(g(x)), \\ g(x) &= w^T \Phi(x) + b, \end{aligned} \tag{11}$$

where $g(x)$ is the functional margin, $\Phi(x)$ is the SVM kernel feature mapping from $\Re^{\flat} \rightarrow \Re^{\flat}$ [more info about the kernel selection can be referred from Jebara (2004)], $\{w, b\}$ is the hyperplane that separates the data and $w \in \Re^{\flat}$, $b \in \Re$.

Consequently, SVC aims at finding the parameters $\{w, b\}$ for an optimal hyperplane in order to maximize the margin of separation of the training samples. It is determined by acquiring the minimum of geometrical distances of two classified classes. The problem is eventually transformed into:

$$\begin{aligned} \{w, b\} &\leftarrow \arg\min_{w,b,\xi} \frac{1}{2} w^T w + C \sum_{i=1}^{M} \xi_i \\ \text{s.t.} y_i g(x_i) &= y_i (w^T x_i + b) \geq 1 - \xi_i, \forall i \in [1, 2, \ldots, M]. \end{aligned} \tag{12}$$

Equation (12) is solved through the method of Lagrange multipliers (Jebara 2004) by defining the Lagrange function. C is regularization parameter that decides the tradeoff between training error and generalization ability, and ξ_i is the slack variables representing the upper and lower constraints of the margin. Then Eq. (12) and its derivation conditions are eventually transformed into the convex quadratic programming optimization as shown in Eq. (13).

$$\begin{aligned} \{w, b\} &\leftarrow \arg\max_{\alpha} \Psi(\alpha, x) \\ \Psi(\alpha, x) &= \sum_{i=1}^{M} \alpha_i - \frac{1}{2} \sum_{i=1}^{M} \sum_{j=1}^{M} \alpha_i \alpha_j y_i y_j d(x_i, x_j) \\ \text{s.t.} \sum_{i=1}^{M} \alpha_i y_i &= 0, 0 \leq \alpha_i \leq C, \end{aligned} \tag{13}$$

where x_i are the determinants for the model, which are called support vectors with corresponding $\alpha_i \neq 0$, and $d(x_i, x_j)$ is the distance between two support vectors.

In conventional SVM cases, $d(x_i, x_j)$ is defined as the Euclidean distance when all features are evenly considered. However for the IE signal, some features from FFT or DWT could have different influence to determinate the analysis of the signal. Thus it's promising to use distance metric learning (ML) to learn the adaptive distance metric according for different classes and features.

We propose to use the ML-SVM approach to learning a Mahalanobis metric between the support vectors, which can be defined with a positive semi-definite matrix $A \succeq 0$ called Mahalanobis distance matrix:

$$d_A(x_i, x_j) = (x_i - x_j)^T M (x_i - x_j). \tag{14}$$

A desirable metric distance is the one preserves the same class as a small margin in the distance space. By introducing the Mahalanobis metric, ML models the constraint Eqs. (12) and (13) as a semi-definite programming (SDP) optimization problem.

$$\begin{aligned} \text{learn}\{\mathrm{A}, \xi\} &\leftarrow \arg\min_{\mathrm{A} \succeq 0, \xi \geq 0} \frac{\lambda}{2} \|\mathrm{A}\|_{\mathrm{F}}^2 + \frac{1}{\mathrm{M}} \sum_{\mathrm{i}=1}^{\mathrm{M}} \xi_{\mathrm{i}} \\ d_A(x_i, x_k) - d_A(x_i, x_j) &\geq 1 - \xi_{ijk}, \forall (i, j, k) \in S_i, \end{aligned} \tag{15}$$

where $S_i = \{(i, j, k), y_i = y_j, y_i \neq y_k\}$ is the neighbor set of x_i. $\|A\|_F^2 = \sum \sum A_{ij}^2$ represents the Frobenius norm for matrix A.

In order to solve the ML-SVM optimization problem in Eq. (15), Pegasos method (Shalev-Shwartz et al. 2011) was applied as an iterative algorithm to solve the SDP via gradient descent.

6 Experiment

The Rise-Rover climbing robot testing is conducted in the Steinman Hall (ST) engineering building at The City College, The City University of New York. The specification of the robot is elaborated upon in Sect. 6.1. The maneuverability is evaluated in a series of surfaces, including smooth ground surfaces, smooth wall surfaces, normally smooth wall surfaces, and rough concrete wall surfaces. In addition, the material tests, high-speed brushless DC tests and noise tests are also performed with quantitative evaluation.

The IE data field collection was conducted for a bridge located at Flushing 149st between Barton Ave and 41st Ave, New York City, as shown in Fig. 13. This bridge was found with visible cracks and possible invisible flaws in the deck. The NDE Rise-Rover climbing robot was placed on both the bridge deck to collect the IE signals, with the robot odometry providing the location of each inspection points. To build the ground truth for the bridge concrete flaw classification of the IE signals, a civil engineer of IE empirical analysis performed a full evaluation on the field samples, and 800 samples of high empirical analysis

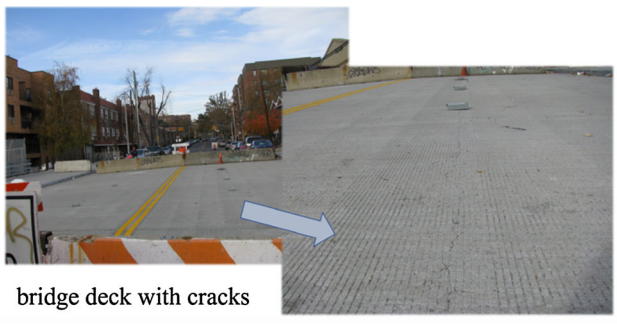

Fig. 13 The Concrete bridge for NDE Rise-Rover field testing, which is located at Flushing 149st in New York City

certainty were further evaluated by the conventional SVM, and ML-SVM with FFT and DWT analysis.

6.1 Rise-Rover climbing robot testing

The performance of the Rise-Rover is evaluated and the specifications are summarized as follows:

Dimension of each drivetrain module: 8 inches × 21 inches × 5.5 inches.
The maximum normal suction force generated by each module: 30 lbs.
Whole unit self-weight (two drivetrain modules plus payload chamber): 24 lbs.
Pull-up force (i.e., payload carrying on vertical wall): 16 lbs.
Locomotion speed: 30 m/min.
Power consumption: Peak 4 KWh.
The Rise-Rover test videos can be seen at:[2] and.[3]

6.1.1 Maneuverability test

The maneuverability of Rise-Rover was revealed in various types of the wall surfaces, which includes: smooth ground surface,[4] smooth wall surface,[5] normally smooth wall surface (with small gaps),[6] and rough concrete wall surface (with big gaps).[7] The designed Rise-Rover is also capable of transiting from the ground to the surface wall.[8] Experiment of climbing in different directions, rotations and overcoming gasp are carried out on the surface walls as well. However in current stage, the Rise-Rover might detach the wall surface when performs the wall transition, so a re-adhesion mechanism using ducted fans is designed to cope with this failure, then the robot is able to recover the adhesion.

Figure 14 shows the maximum payload test on a vertical smoothness surface in an indoor environment in ST building.

6.1.2 Material test

Part of the challenge of developing the Rise-Rover wall-climbing robot is to find good tread material. The tread shall be durable against tear and wear, and yet soft and conformable enough to overcome surface irregularities in order to generate strong suction force. We tested over a dozen samples, from foams to gels and even a rubber tread. A tread with no suction will not stick on a wall; but too much suction will prevent the robot from climbing the wall. We used a specially designed experimental setup on which we tested our tread materials on three different contact surfaces (cinder block surface, painted block wall surface, and smooth plexiglass surface).

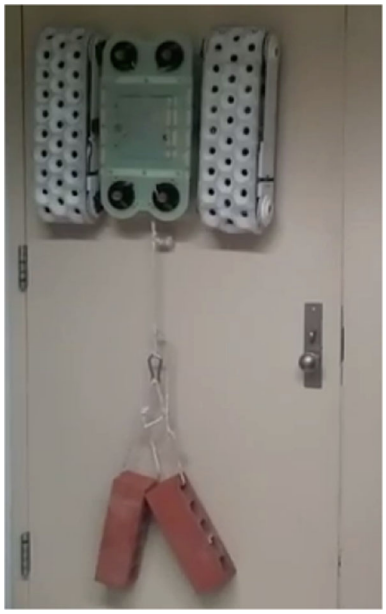

Fig. 14 Rise-Rover (with white wheel tread) with 7 kg payload test on a smooth door

The experimental data shows that there is no single material sample that performed the highest in all four categories for any surface/voltage combination. But comparing statistic data, the Silicone Rubber sample generally performed towards the top with no low stats. In addition, its coefficient of friction was very consistent. We eventually selected to use two materials: light-weight foam material covered by silicone rubber to reduce weight. We have developed a molding procedure to produce the tread that uses light-weight foams encapsulated by silicone rubber. The tread is durable against tear and wear, and it's able to overcome surface irregularities to generate strong suction.

6.1.3 High-speed brushless DC test

To achieve higher speed for the vacuum motor, couple of testing are carried out to select the best sample period setting. The stability of the speed control is maintained by setting the shaft angle. As shown in the following table, it is the shaft angle setting time in different Rotations per Minute (RPM). Table 2 shows the high-speed DC sample period setting for the timer for various RPM.

[2] https://www.youtube.com/watch?v=5flaoIwEZFM
[3] https://www.youtube.com/watch?v=Cz8U9M19agA
[4] https://www.youtube.com/watch?v=Cz8U9M19agA#t=0m38s
[5] https://www.youtube.com/watch?v=5flaoIwEZFM#t=0m57s
[6] https://www.youtube.com/watch?v=Cz8U9M19agA#t=1m07s
[7] https://www.youtube.com/watch?v=Cz8U9M19agA#t=1m40s
[8] https://www.youtube.com/watch?v=5flaoIwEZFM#t=0m25s

Table 2 High-speed DC sample period setting

RPM	RPS	Cycle(us)	Half of cycle(us)	Half of cycle/25	Half of cycle/10	Half of cycle/5	TMR
5000	83.3	12,000	6000	240	600	1200	33,149
10,000	166.7	6000	3000	120	300	600	16,575
20,000	333.3	3000	1500	60	150	300	8287
40,000	666.7	1500	750	30	75	150	4144
60,000	1000	1000	500	20	50	100	2762
80,000	1333.3	750	375	15	38	75	2072
100,000	1666.7	600	300	12	30	60	1657

6.1.4 Noise test

We found out that the major source of noise is from the suction rotor package that consists of the high-speed motor and impeller blade. The diagnosis indicates that the high frequency noise is caused either by a misalignment in assembly and/or unbalanced impeller blade. The manufacturer must have impeller balancing procedure in place to ensure correct blade spacing, equal blade thickness, balanced weight, etc. We also noticed some tricks in impeller design to make balancing easy in the Roomba from the iRobot and Dyson vacuum cleaners. The measurement data show that Rise-Rover generates noise in the range of 67.4, 69.3, 72.9 db at three different power levels. The Dyson vacuum cleaner generates noise at 70.2, 75.8 db in low/high power levels. The AC vacuum motor generates noise at 75.3, 80.3, and 82.1 db when the voltage is set to 40, 60, and 80 V respectively. The signal-to-noise ratio (SNR) in different levels were analyzed for the high-frequency vibration noise, which then was filter out by the low-pass filter. The conclusion is that the noise from Rise-Rover is not a big issue, and it is actually slightly lower than the commercial counterpart.

6.2 IE analysis evaluation

The IE signals were collected by the IE device from impact-echo Instruments, LLC as shown in Fig. 3. To release the noise affect, the typical noises from the field test were collected with our the NDE impact, more details are as shown in Sect. 6.1.4. The high-frequency vibration noises were filtered out so that the proposed method can be applied in the noisy environments.

To ensure the selected DWT components approximating the original signal, we performed the DWT decomposition on the IE signal. Figure 15 shows the comparison of original and reconstructed signals from DWT main components (cA_4, cD_4, cD_3). From the top part of Fig. 15, we can see that the reconstructed signals of DWT main components are capable of representing the original signal in most of the time domain with residue ϵ. As shown in the bottom part of Fig. 15, for a typical IE signal among the tested samples, we got the residue $\epsilon \leq 0.09$, which is the

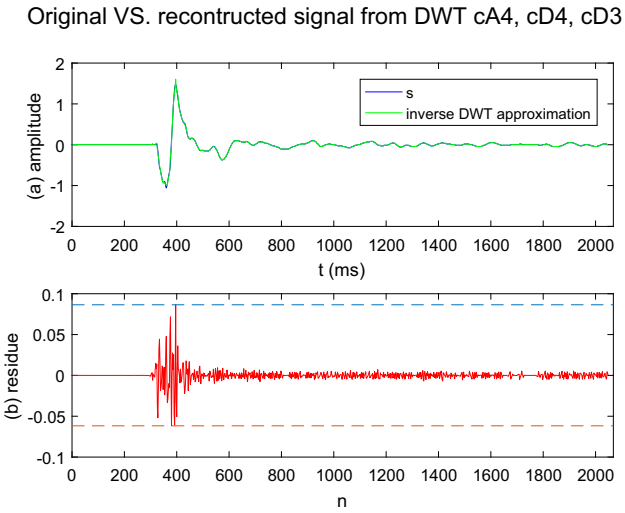

Fig. 15 Original Vs. reconstructed signal from DWT main components

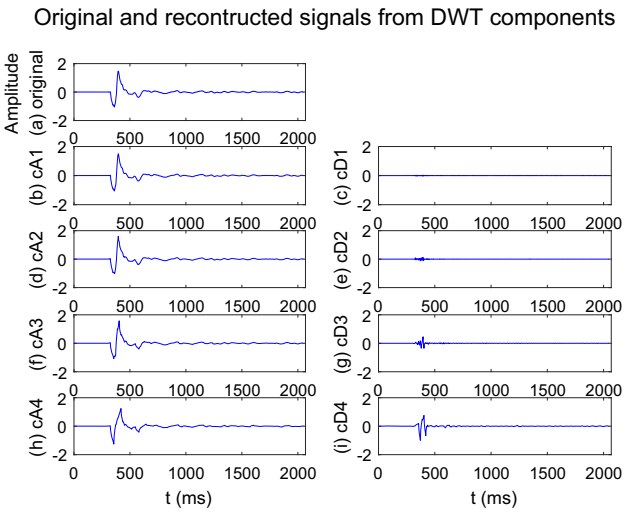

Fig. 16 IE signal DWT decomposition components

rate of 5.63% w.r.t the amplitude of the original signals. Thus the residue is negligible and the selected main components of the DWT maintain the characteristics of the original IE signal. The IE signal DWT decomposition components are as shown in Fig. 16.

Figure 17 shows the TD, FFT and PSD of original signal and DWT main components (cA_4, cD_4, cD_3).

The field collected samples were evaluated by a civil engineer with the IE empirical analysis. It's the PSD in the frequency domain of the IE signal that contains the information of inner defects or flaws, which can be in various forms such as cracks, voids. To ensure the empirical analysis as the ground truth, we classified the samples with only two categories of flaw and non-flaw. With the uneven distribution on the PSD, it's can be easily classified by the empirical analysis. We selected 800 samples from IE inspection samples on the concrete bridge deck. To verify the performance on the field tested bridge deck for the wall-climbing robot, the field samples were divided into two sets for the training and evaluation as 650 and 150 respectively. The empirical analysis of the concrete bridge deck is shown in the Table 3.

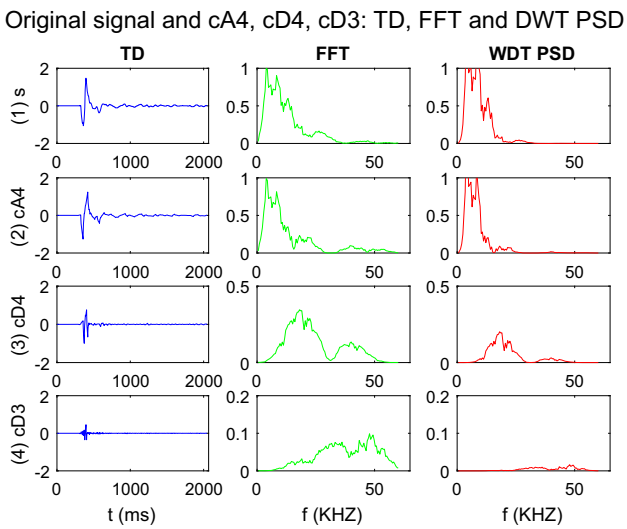

Fig. 17 TD, FFT and PSD of original signal and DWT cA_4, cD_4, cD_3

Table 3 Empirical analysis for concrete bridge deck datasets

Category	Samples	Rate (%)
Non-flaw samples in training set	538	82.8
Flaw samples in training set	112	17.2
Non-flaw samples in test set	131	87.3
Flaw samples in test set	19	12.7

To automate the analysis of IE acoustic sound, the training data sets are used to train the SVM model and then the model is evaluated by the test data set. The data analysis tasks of preprocessing, FFT, DWT and ML-SVM training and evaluation are performed using MATLAB.

After the training procedure, the SVM classifier was verified with the test dataset. To illustrate the performance of the ML-SVM methodology, the result was compared with the outcome from empirical analysis and conventional SVM in our previous research of the IE NDE signals. The test data set was classified by the ML-SVM model. Table 4 shows the comparison of empirical, SVM, and ML-SVM result, for the results of the detected flaw, true negative (TN), true positive (FP), false negative (FN), false positive (FP). As we can see that the ML-SVM detected flaws 13.3% is more closer to 12.7% from empirical analysis in Table 3, comparing with SVM detected flaws 14.7%. It has a 90% for the TN for the detected flaws which performs better than the conventional SVM as 77.3% applied in our previous research (Li et al. 2014), and 99.2% for the TP for the detected non-flaws while SVM as 98.4%. Clearly that ML-SVM improves the TN significantly by using multiple features from FFT and DWT for the SVM binary classification model.

After we evaluated all the data sets, we visualized the IE signal in both forms of B-Scan and volumetric view. Figure 18 shows the classification results in a detected line area, where the IE motion platform moves in the horizontal line with the range of 40 cm, and 20 IE samples were recorded for the B-Scan visualization. The vertical show the depth of the concrete and it's corresponding to the spectrum of founded flaws. Figure 19 shows the volumetric view of the whole test samples, where the IE motion platform is with the range of 40 cm, and the robot moves forward with the range of 160 cm, and the grids of 10×20

Table 4 Comparison of different approaches

Category	Empirical samples	Empirical analysis (%)	SVM samples	SVM rate (%)	ML-SVM samples	ML-SVM rate (%)
Detected flaws	19	12.7	22	14.7	20	13.3
TN	19	100	17	77.3	18	90.0
TP	131	100	126	98.4	129	99.2
FN	N/A	N/A	2	1.6	1	0.8
FP	N/A	N/A	5	22.7	2	10.0

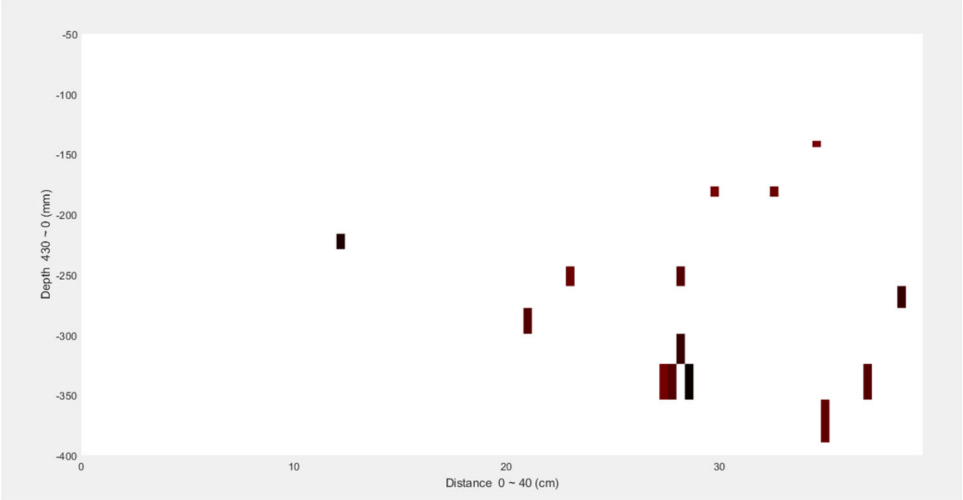

Fig. 18 2D B-Scan view of a subset samples

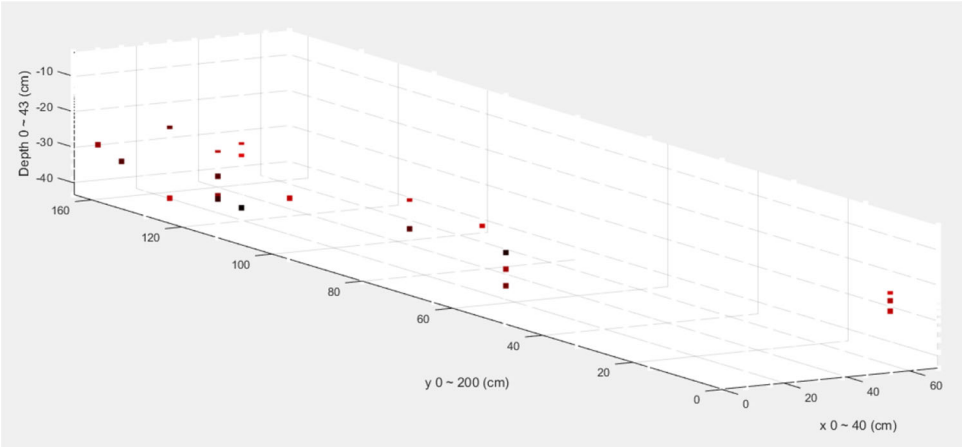

Fig. 19 Volumetric view of ML-SVM classified IE flaws

are used to detected the IE samples. The group position of some detected points in the space can also indicate a high possibility of flaws existing in the corresponding positions of the inner bridge deck.

7 Conclusion

We proposed a novel wall-climbing robot (Rise-Rover) which is equipped with an IE device, to perform NDE on concrete structures based on FFT, WT and Metric learning SVM. A novel vacuum suction module was newly designed in the caterpillar chain-tracks wheels of the robot to maintain adhesion reliability while ensuring the locomotion mobility. With the self-weight 24 lbs, the Rise-Rover can carry 16 lbs on vertical wall at the locomotion speed of 30 m/min. The IE signals were automatically analyzed using both Fourier transform and Wavelet transform, then the features were extracted based on the power spectral density statistics, and a distance ML-SVM approach was applied for the automatic classification. The experiment shows that the Rise-Rover works effectively on the vertical surface with small gaps or ditches. Future research will focus on reducing the mechanical weight of the motion platform so that it can perform inspection on vertical concrete plates, and use other modalities (such as vision, or GPR) of NDE for automatic inspection.

Acknowledgements This research was supported by US National Science Foundation (NSF) I-Corps program and The Small Business Technology Transfer (STTR) Phase-1 grant: Wall-climbing Robots for Nondestructive Inspection to Ensure Sustainable Infrastructure, and US Department. of Transportation (RITA/USDOT) Grant 49997-41-24: Robotic Inspection of Bridges Using impact-echo Technology. The authors would like to thank Dr. Anil Agrawal and Dr. Hongfan Wang at the Department of Civil Engineering, The City College of New York, for providing guidance on empirical analysis for our experiment on impact-generated stress wave on the concrete bridge.

References

Bi, Z., Guan, Y., Chen, S., Zhu, H., Zhang, H.: A miniature biped wall-climbing robot for inspection of magnetic metal surfaces. In: Robotics and Biomimetics (ROBIO), 2012 IEEE International Conference on, IEEE, pp. 324–329. (2012)

Carino, N.J., et al.: The impact-echo method: an overview. In: Proceedings of the 2001 Structures Congress & Exposition, pp. 21–23 (2001)

Daniels, J.J., et al.: Ground penetrating radar fundamentals, pp. 1–21. Region V, Prepared as an appendix to a Report to the US EPA (2000)

Farrar, C.R., Worden, K.: Structural Health Monitoring: A Machine Learning Perspective. Wiley, New York (2012)

Galt, S., Luk, B., Cooke, D., Collie, A.: A tele-operated semi-intelligent climbing robot for nuclear applications. In: Mechatronics and Machine Vision in Practice, 1997. Proceedings., Fourth Annual Conference on, IEEE pp. 118–123 (1997)

Guan, Y., Zhu, H., Wu, W., Zhou, X., Jiang, L., Cai, C., Zhang, L., Zhang, H.: A modular biped wall-climbing robot with high mobility and manipulating function. IEEE/ASME Trans. Mech. **18**(6), 1787–1798 (2013)

Gucunski, N., Maher, A.: Evaluation of seismic pavement analyzer for pavement condition monitoring. Technical report (2002)

Hao, S.: I-35w bridge collapse. J. Bridge Eng. **15**(5), 608–614 (2009)

Harley, J.B.: Data-driven, sparsity-based matched field processing for structural health monitoring. (2014)

Ito, Y., Uomoto, T.: Nondestructive testing method of concrete using impact acoustics. NDT E Int. **30**(4), 217–222 (1997)

Jebara, T.: Multi-task feature and kernel selection for svms. In: Proceedings of the twenty-first international conference on Machine learning, ACM, p. 55 (2004)

Li, B., Cao, J., Xiao, J., Zhang, X., Wang, H.: Robotic impact-echo non-destructive evaluation based on fft and svm. In: Intelligent Control and Automation (WCICA), 2014 11th World Congress on, IEEE, pp. 2854–2859 (2014)

Liu, Y., Caselles, V.: Improved support vector machines with distance metric learning. In: International Conference on Advanced Concepts for Intelligent Vision Systems, pp. 82–91. Springer (2011)

Liu, D., Dissanayake, G., Miro, J.V., Waldron, K.: Infrastructure robotics: Research challenges and opportunities. In: ISARC. Proceedings of the International Symposium on Automation and Robotics in Construction, vol. 31, p. 1. Vilnius Gediminas Technical University, Department of Construction Economics and Property (2014)

Liu, K.P., Luk, B.L., Yeung, T.W., Tso, S.K., Tong, F.: Wall inspection system for safety maintenance of high-rise buildings. Int. J. Perform. Eng. **3**(1), 187 (2007)

Liu, P.L., Yeh, P.L.: Imaging Methods of Concrete Structure Based on Impact-Echo Test. INTECH Open Access Publisher, Rijeka (2012)

Liu, P.L., Yeh, B.L., Yiu, C.Y.: Imaging of concrete defects using elastic wave tests. Bull Coll Eng, NTU **91**, 41–50 (2004)

Luk, B.L., Liu, K., Jiang, Z., Tong, F.: Robotic impact-acoustics system for tile-wall bonding integrity inspection. Mechatronics **19**(8), 1251–1260 (2009)

McCann, D., Forde, M.: Review of ndt methods in the assessment of concrete and masonry structures. NDT E Int. **34**(2), 71–84 (2001)

Mur-Artal, R., Tardós, J.D.: ORB-SLAM2: an open-source SLAM system for monocular, stereo and RGB-D cameras. IEEE Trans Robot (2017)

Nguyen, N., Guo, Y.: Metric learning: A support vector approach. In: Joint European Conference on Machine Learning and Knowledge Discovery in Databases, pp. 125–136. Springer (2008)

Olson, L.D.: Innovations in bridge superstructure condition assessment with sonic and radar methods. Struct. Mater. Technol. 2010 (2010)

Pratt, D., Sansalone, M.: Impact-echo signal interpretation using artificial intelligence. Mater. J. **89**(2), 178–187 (1992)

Sansalone, M.J., Streett, W.B.: Impact-echo. nondestructive evaluation of concrete and masonry (1997)

Sardy, S., Tseng, P., Bruce, A.: Robust wavelet denoising. IEEE Trans. Signal Process. **49**(6), 1146–1152 (2001)

Shalev-Shwartz, S., Singer, Y., Srebro, N., Cotter, A.: Pegasos: primal estimated sub-gradient solver for svm. Math. Program. **127**(1), 3–30 (2011)

Short, R., Fukunaga, K.: The optimal distance measure for nearest neighbor classification. IEEE Trans. Info. Theory **27**(5), 622–627 (1981)

Srivastava, A.N., Han, J.:: Machine Learning and Knowledge Discovery for Engineering Systems Health Management. CRC Press, Boca Raton (2011)

Strickland, E.: Crawler bot could inspect nuclear power stations. IEEE Spectr. (2013)

Tan, K., Chan, K., Wong, B., Guan, L.: Ultrasonic evaluation of cement adhesion in wall tiles. Cem. Concr. Compos. **18**(2), 119–124 (1996)

Tong, F., Xu, X., Luk, B., Liu, K.: Evaluation of tile-wall bonding integrity based on impact acoustics and support vector machine. Sens. Actuators A Phys. **144**(1), 97–104 (2008)

Ward, P., Liu, D., Waldron, K., Hasan, M.: Optimal design of a magnetic adhesion for climbing robots. In: Proceedings of the 16th international conference CLAWAR-2013 on nature-inspired mobile robotics, Sydney, Australia, pp. 375–382. World Scientific Publishing (2013)

Wu, H., Siegel, M.: Correlation of accelerometer and microphone data in the coin tap test. IEEE Trans. Instrum. Meas. **49**(3), 493–497 (2000)

Xiao, J., Agrawal, A.: Robotic inspection of bridges using impact-echo technology. UTRC-RITA Project Final Report (2015)

Xiao, J., Calle, A., Sadegh, A., Elliott, M.: Modular wall climbing robots with transition capability. In: 2005 IEEE International Conference on Robotics and Biomimetics-ROBIO, pp. 246–250. IEEE (2005)

Xiao, J., Li, B., Ushiroda, K., Song, Q.: Rise-rover: A wall-climbing robot with high reliability and load-carrying capacity. In: Assistive Robotics: Proceedings of the 18th International Conference on CLAWAR 2015, World Scientific, p. 299 (2015)

Xiao, J., Morris, W., Chakravarthy, N., Calle, A.: City climber: a new generation of mobile robot with wall-climbing capability. In: Proceedings of SPIE, vol. 6230, p. 62301d. (2006)

Xiao, J., Sadegh, A., Elliot, M., Calle, A., Persad, A., Chiu, H.M.: Design of mobile robots with wall climbing capability. Proceedings of IEEE AIM, pp. 438–443. Monterey, CA (2005)

Xiao, J., Wang, H.: Contemporary issues in systems science and engineering (chapter22: Advances in climbing robots) (2015)

Xiao, J., Sadegh, A.: City-Climber: A New Generation Wall-Climbing Robots. INTECH Open Access Publisher, Rijeka (2007)

Xing, E.P., Ng, A.Y., Jordan, M.I., Russell, S.: Distance metric learning with application to clustering with side-information. Adv. Neural Info. Process. Syst. **15**, 505–512 (2003)

Yeh, P.L., Liu, P.L.: Application of the wavelet transform and the enhanced fourier spectrum in the impact echo test. NDT E Int. **41**(5), 382–394 (2008)

Ying, Y., Garrett Jr., J.H., Oppenheim, I.J., Soibelman, L., Harley, J.B., Shi, J., Jin, Y.: Toward data-driven structural health monitoring: application of machine learning and signal processing to damage detection. J. Comput. Civil Eng. **27**(6), 667–680 (2012)

Zhang, J.K., Yan, W., Cui, D.M.: Concrete condition assessment using impact-echo method and extreme learning machines. Sensors **16**(4), 447 (2016)

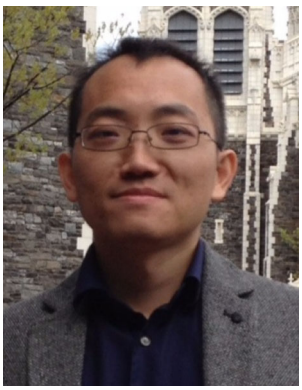

Bing Li is a Ph.D student in CCNY Robotics Lab at the Department of Electrical Engineering of The City College, City University of New York. He received his M.E, and B.E. degree from Beihang University and Beijing Forestry University, Beijing, China, in 2009 and 2006 respectively. His research interests include assistive robotics, indoor navigation, robotic NDE inspection, machine learning, and 3D SLAM.

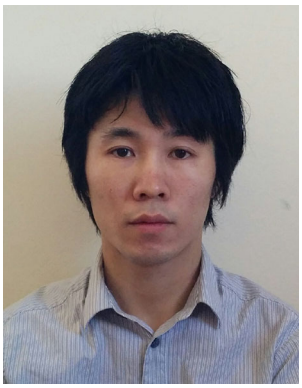

Kenshin Ushiroda received a Mechanical Engineering degree from The City College, The City University of New York in 2013. After receiving the NSF Phase I SBIR grant, he worked to develop a wall climbing machine at the CCNY Robotics Lab as the principle investigator. He was employed in 2017 at 3D Platforms as a Mechanical Design Engineer to help develop and produce a high volume flow filament extruder for their 3D printers.

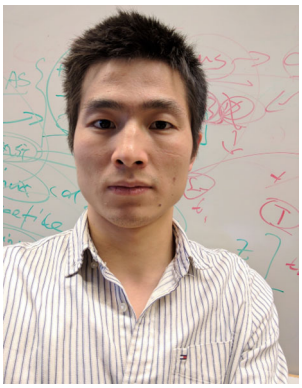

Liang Yang is a Ph.D student at The City College, City University of New York, and Ph.D candidate of State Key Laboratory of Robotics, University of Chinese Academy of Sciences. He received his bachelor degree from Shenyang Aerospace University in 2012. From 2015, he works as research assistant at the Robotics Lab at the City College of New York. He is currently working at CCNY Robotics Lab, he focuses on visual navigation, SLAM, visual inspection based on deep learning approach, and unmanned system.

Qiang Song received a MS degree in control theory and control engineering from Taiyuan University of Technology. From 2006 to 2012, He worked as an associate professor in Taiyuan Institute of Electrical Engineering. From 2010 to 2011. He worked as a visiting scholar in The City College, The City University of New York. His research focuses on the real-time embedded system, motion algorithm and control, circuit design etc.

Jizhong Xiao is a full professor at the Department of Electrical Engineering at The City College, City University of New York, where he has directed the CCNY Robotics Lab since 2002. He received B.S. and M.S from East China Institute of Technology in 1990 and 1993 respectively, a M.Eng. from Nanyang Technological University, Singapore in 1999, and a Ph.D. from Michigan State University in 2002, His research interests include the wall-climbing robots, Micro-UAV, assistive navigation, and 3D SLAM.